


 Cite this: *RSC Adv.*, 2022, **12**, 24596

Synthesis of polyaspartic acid-capped 2-aminoethylamino acid as a green water treatment agent and study of its inhibition performance and mechanism for calcium scales†

 Yong-Hong Cai,^a Jia-Li Zhao,^a Xin-Yu Guo,^{ab} Xiao-Juan Zhang,^a Ran-Ran Zhang,^a Shao-Rong Ma,^a Ya-Min Cheng,^{ID *a} Zhong-Yan Cao,^{ID *a} and Ying Xu,^{ID *abc}

Polyaspartic acid (PASP), a well-known green scale inhibitor for industrial water treatment, might be decomposed with prolonged duration, and its anti-scaling performance against CaCO_3 and CaSO_4 is diminished at a low concentration ($<10 \text{ mg L}^{-1}$) and a high temperature. With semi-ethylenediaminetetraacetic acid (EDTA) tetrasodium salt as the mimicking model, novel phosphorus-free PASP-capped 2-aminoethylamino acid (PASP-ED₂A) containing side chains bearing multi-functional groups is rationally designed and successfully prepared *via* the ring-opening reaction of cheap poly(succinimide) under mild reaction conditions with the assistance of readily available 2-aminoethyl amino acid. The static scale inhibition method is used to evaluate the scale inhibition performance of the as-synthesized PASP derivative. Scanning electron microscopy, X-ray diffraction, and X-ray photoelectron spectroscopy are utilized to monitor the crystallization process of calcium carbonate and calcium sulfate scales, and density functional theory calculations are conducted to shed light on the relationship between the molecular structure and scale inhibition mechanism of PASP-ED₂A. Results show that the as-prepared PASP-ED₂A shows better scale inhibition performance for CaCO_3 and CaSO_4 than PASP with a low concentration, a high temperature, and an extended duration. Particularly, PASP-ED₂A with a concentration of 10 mg L^{-1} exhibits the best scale inhibition performance for CaCO_3 ; its scale inhibition capacity is about two times as much as that of PASP. The reason lies in that the coordination atoms in the molecular structure of PASP-ED₂A can chelate with Ca^{2+} to inhibit the combination of Ca^{2+} with anions and prevent the generation of CaCO_3 and CaSO_4 scales. The PASP-ED₂A derivative can more efficiently retard the formation and growth of CaCO_3 and CaSO_4 crystal nuclei and exerts better inhibition performance against CaCO_3 and CaSO_4 scales than PASP.

 Received 1st July 2022
 Accepted 23rd August 2022

DOI: 10.1039/d2ra04075a

rsc.li/rsc-advances

1. Introduction

With the rapid development of industry and the increase of water consumption,¹ water recycling has become an important means to save water resources. Reports demonstrate that industrially circulated cooling water accounts for 70–90% of the total industrial water consumption.² However, the repeatedly used cooling water often contains increased contents of calcium and magnesium ions and is hence liable to scaling.^{3,4} This will not only cause the clogging and corrosion of heat exchange and

production equipment but also reduce the heat transfer rate of the equipment, thereby adding to the production cost.^{5–9} Therefore, some researchers developed several techniques for inhibiting or remediating the scale formation and found that scale inhibitors could be of special significance in this respect.^{10–13} Among various scale inhibitors, polyaspartic acid (PASP) could be the most promising one, since it is cheap, non-toxic, phosphorous-free and biodegradable.^{14–18} Nevertheless, it exhibits relatively poor scale inhibition performance at a low concentration or high temperature over a prolonged duration, which limits its practical application in industry.¹⁹ In this sense, it is imperative to design and synthesize phosphorus-free PASP derivatives with desired antiscale performance under mild reaction condition. Two major strategies are currently available for that purpose. One is the copolymerization of L-aspartic acid, and another is the amino ring-opening modification of poly-succinimide (PSI). Both strategies afford functionalized PASP

^aCollege of Chemistry and Chemical Engineering, Henan University, Kaifeng 475004, China. E-mail: chengyamin@henu.edu.cn; zycao@henu.edu.cn; hdccxu@126.com

^bEngineering Research Center for Water Environment and Health of Henan, Zhengzhou University of Industrial Technology, Zhengzhou 451150, China

^cCentral Philippine University, Iloilo 5003, Philippines

† Electronic supplementary information (ESI) available. See <https://doi.org/10.1039/d2ra04075a>



with improved antiscalting efficiency, thanks to the introduction of the side chains bearing functional groups (e.g., sulfonic ($-\text{SO}_3\text{H}$), carboxylic ($-\text{CO}_2\text{H}$), hydroxyl ($-\text{OH}$), and amino ($-\text{NR}_2$)) that can be coordinated with Ca^{2+} (Scheme 1).^{20–22}

In practice, however, high concentrations of PASP derivatives are often necessary in order to achieve a satisfactory scale inhibition effect. Viewing that polymers with high chelation ability with Ca^{2+} might contribute to enhancing the antiscalting performance, we envision the selective installation of side chains bearing polydentate coordination groups (carboxylic, amino, acylamido, etc.) might provide a new solution to further improve the scale inhibition performance. Since ethylenediaminetetraacetic acid (EDTA) tetrasodium salt is a very good chelating agent widely used for the quantitative detection of Ca^{2+} , we anticipate that the installation of semi-EDTA to the side chain of the PASP derivative could provide novel antiscalting agents with greatly improved antiscaling performance. With our continuing interest in this area, in the present research we prepare a PASP derivative bearing side chain containing multi-functional group (phosphorus-free PASP-capped 2-aminoethyl amino acid (denoted as PASP-ED₂A)) by mimicking semi-EDTA under mild reaction condition (Scheme 1). This paper evaluates the scale inhibition performance of the as-synthesized PASP derivative by static scale inhibition method and observes the crystallization process of calcium scale by means of scanning electron microscopy, X-ray diffraction, and X-ray photoelectron spectroscopy. Besides, it aims at shedding light on the plausible scale inhibition mechanism of the PASP derivative based on density functional theory (DFT) calculations.

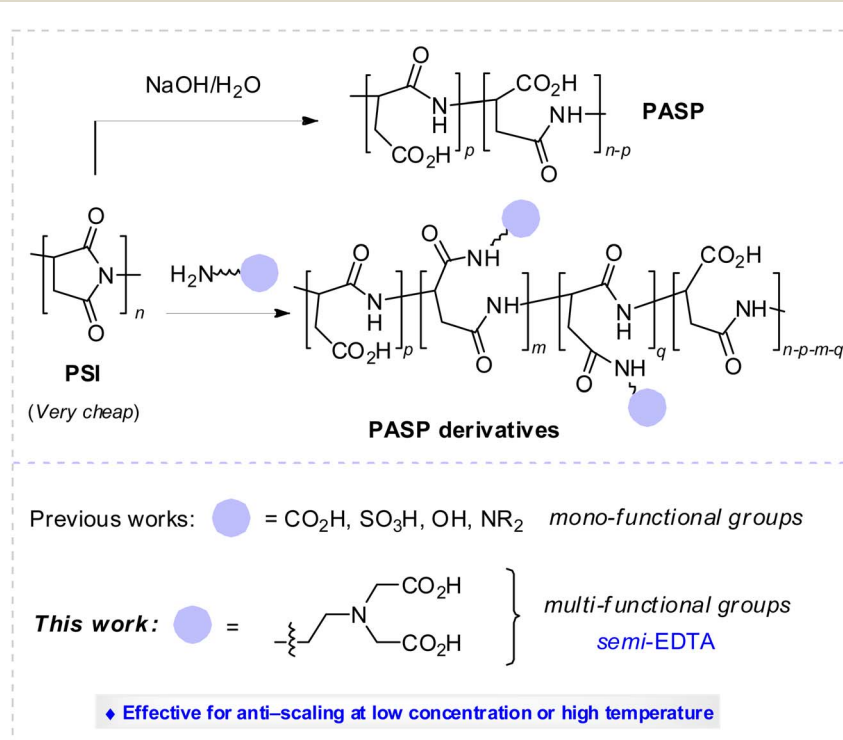
2. Materials and methods

2.1 Materials

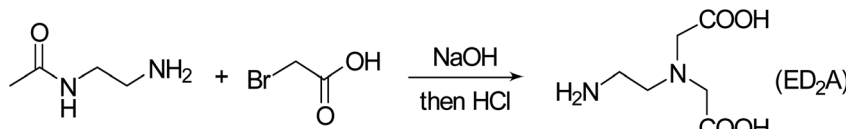
Analytical reagents (AR) bromoacetic acid and ethylenediamine as well as industrial grade PSI ($M_w = 7000$) were provided by Shanghai Aladdin Biochemical Technology Company Limited (Shanghai, China). *N*-Acetylenediamine was purchased from Shanghai Shaoyuan Regent Company Limited (Shanghai, China). Anhydrous sodium sulfate (AR), ethylenediaminetetraacetic acid disodium salt (AR), anhydrous calcium chloride (AR), borax (AR) and potassium hydroxide (AR) were provided by Tianjin Kermel Chemical Reagent Company Limited (Tianjin, China). Anhydrous sodium bicarbonate (AR) was purchased from Tianjin Deen Chemical Regent Company Limited (Tianjin, China). Anhydrous ethanol (AR) was obtained from Anhui Ante Food Company Limited (Suzhou, China). Deionized water (DI) prepared at our laboratory was used as the solvent and for rinsing as well.

2.2 Synthesis of 2,2'-(2-aminoethyl)azanediyi diacetic acid-polyaspartic acid (PASP-ED₂A)

Certain amounts of *N*-acetylenediamine, bromoacetic acid and distilled water were placed in a 50 mL round bottom flask while a proper amount of sodium hydroxide solution (8 mol L⁻¹) was dropwise added. The resultant solution was held at ambient condition for 3 days, followed by the addition of a proper amount of sodium hydroxide solution (5 mol L⁻¹) and further reaction for additional 3 days. Upon completion of reaction, hydrochloric acid (5 mol L⁻¹) was added to adjust the solution pH to about 8 thereby affording ED₂A (Fig. 1).²³



Scheme 1 Synthesis of PASP derivative by ring-opening reaction of polysuccinimide.

Fig. 1 Synthesis route of ED₂A.

Certain amounts of the aqueous solutions of PSI, ED₂A and sodium hydroxide were placed in a 50 mL round bottom flask and stirred at 60 °C for 24 h in a water bath. At the end of reaction, the solution was poured in anhydrous ethanol to allow sedimentation, followed by holding at ambient condition as well as filtration and drying of the lower precipitate to obtain the crude product. The crude product was purified with a dialysis bag and then steamed to obtain a yellow solid, the target product PASP-ED₂A with 53% yield (Fig. 2). Noteworthy, although seven days and extra industrial raw chemical reagents (such as ethylenediamine and bromoacetic acid) was needed to synthesis PASP-ED₂A than that of PASP, the safe and easy-to-handle nature, as well as its better antiscaling performance makes it worth to do.

2.3 Characterization of PASP and PASP-ED₂A

The structure of PASP and PASP-ED₂A was characterized by Fourier transform infrared spectroscopy (VERTEX 70 FTIR spectrometer, Bruker Optics, Germany) and ¹H nuclear magnetic resonance spectroscopy (¹H NMR; AVANCE 400 MHz NMR spectrometer, Bruker Optics, Germany).

2.4 Static scale inhibition tests

2.4.1 Static scale inhibition efficiency against CaCO₃. The static scale inhibition method was used to determine the scale inhibition performance of the as-synthesized PASP-ED₂A derivative as water treatment agent. The test solution containing 240 mg L⁻¹ Ca²⁺ and 732 mg L⁻¹ HCO₃⁻ was prepared and heated at 80 °C for 10 h in a water bath. At the end of heating, the solution was naturally cooled to room temperature. The concentration of Ca²⁺ in the supernatant is determined by EDTA titration. The scale inhibition rate for CaCO₃ is calculated by formula (1):

$$\eta = \frac{C_2 - C_1}{C_0 - C_1} \times 100\% \quad (1)$$

where C_0 is the concentration of Ca²⁺ (mg L⁻¹) in the solution before the experiment, and C_1 and C_2 are the concentrations of Ca²⁺ (mg L⁻¹) in the solutions after the experiments with and without PASP-ED₂A derivative. All the static inhibition tests were conducted in triplicate to ensure reproducibility.

2.4.2 Static scale inhibition efficiency against CaSO₄. The test solution containing 2000 mg L⁻¹ Ca²⁺ and 4800 mg L⁻¹ SO₄²⁻ was prepared and heated at 70 °C for 6 h in a water bath. At the end of heating, the solution was naturally cooled to room temperature. After filtration, the concentration of Ca²⁺ in the supernatant is determined by EDTA titration. The scale inhibition rate for CaSO₄ is calculated by formula (2):

$$\eta = \frac{X_2 - X_1}{X_0 - X_1} \times 100\% \quad (2)$$

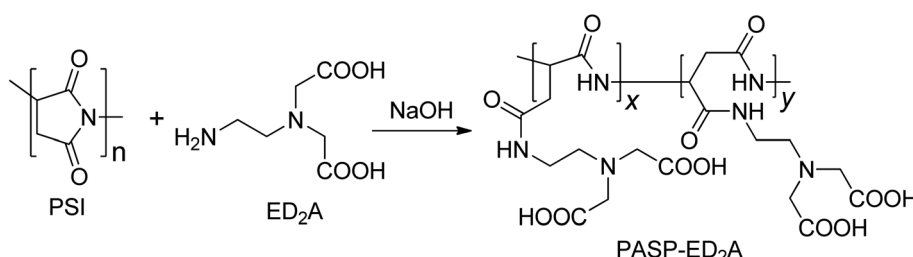
where X_0 is the initial concentration of Ca²⁺ (mg L⁻¹) in the solution before heating; and X_2 and X_1 are the concentrations of Ca²⁺ (mg L⁻¹) after reaction in the presence and absence of the scale inhibitor. The static inhibition tests were repeated for three times; and the averages of the repeat tests were cited to minimize data scattering.

2.5 Surface analysis of scale crystal

A field emission scanning electron microscope (SEM, JSM-7610F, Japan Electronics Corporation) was used to observe the morphology of the scales. An X-ray powder diffractometer (XRD, D8 Advance, Bruker, Germany) was used to analyze the crystalline change of CaCO₃ scale and CaSO₄ scale. An X-ray photoelectron spectroscope (XPS, Thermo Scientific K-Alpha+, USA) was performed to explore the scale inhibition mechanism of PASP-ED₂A derivative.

2.6 Monitoring crystallization process of calcium scale

The pH curve of CaCO₃ solution can reflect the scale inhibition performance of PASP-ED₂A derivative to a certain extent.²⁴ Prior to the experiments, CaCl₂ solution and NaHCO₃ solution of an

Fig. 2 Synthesis route of PASP-ED₂A derivative.

equal concentration were prepared. The as-obtained CaCl_2 solution and NaHCO_3 solution were then mixed at pre-set volume fractions to afford the to-be-tested CaCO_3 solutions with concentrations of 0.015, 0.020, 0.025, and 0.030 mol L^{-1} (denoted as solutions A, B, C, and D). Before the CaCl_2 solution and NaHCO_3 solution were mixed, their pH was adjusted to 8.9 with NaOH solution while the scale inhibitor was added to the NaHCO_3 solution in advance. The mixed solution was stirred at $(25.0 \pm 0.1)^\circ\text{C}$ and its pH was recorded at pre-set time intervals. The time when the pH started to drop sharply is recorded as t_{ind} . According to the theory of classic homogeneous nucleation, the relationship between t_{ind} and $\ln S$ can be obtained from eqn (3):^{25,26}

$$\ln t_{\text{ind}} = B + \frac{\beta \gamma^3 V_m^2 N_A f(\theta)}{R^3 T^3 (\ln S)^2} \quad (3)$$

where B is the constant, γ is the surface energy of calcium carbonate or calcium sulfate crystal (J m^{-2}), β is the geometric (shape) factor of $16\pi/3$ for the spherical nucleus, $f(\theta)$ is the correction factor (1.0 for homogeneous nucleation and <1.0 for heterogeneous nucleation),^{25,28} V_m is the molar volume of the phase forming ($36.93 \text{ cm}^3 \text{ mol}^{-1}$ for CaCO_3 and $74.69 \text{ cm}^3 \text{ mol}^{-1}$ for $\text{CaSO}_4 \cdot 2\text{H}_2\text{O}$),²⁵ N_A is Avogadro's number, R is the gas constant, and T is the absolute temperature.

Similarly, the conductivity test of CaSO_4 solution can reflect the performance of the scale inhibitor to a certain extent. In this case, CaCl_2 solution and Na_2SO_4 solution with the same concentration were prepared in advance; and they were then mixed at pre-set volume fractions to obtain CaSO_4 solutions with concentrations of 0.07, 0.08, 0.09, and 0.10 mol L^{-1} (denoted as solutions A₁, B₁, C₁, and D₁). Before the CaCl_2 solution and Na_2SO_4 solution were mixed, their pH was adjusted to 8.9 with NaOH solution while the scale inhibitor was added to the Na_2SO_4 solution in advance. The mixed solution was stirred at $(25.0 \pm 0.1)^\circ\text{C}$, and its conductivity was recorded at pre-set time intervals. The time when the conductivity started to drop sharply is recorded as t_{ind} . According to the theory of classic homogeneous nucleation, the relationship between t_{ind} and $\ln S$ can also be expressed by eqn (3).^{26,27}

For the pH test of calcium carbonate, the supersaturation ratio (S) of the four tested solutions is 93.325, 144.544, 204.174, and 269.153, respectively, based on the calculation from Yang.²⁹ For the conductivity test of calcium sulfate, the supersaturation ratio (S) of the four tested solutions is 5.248, 6.166, 7.079, and 8.128.

3. Results and discussion

3.1 Structural characterization of PASP and PASP-ED₂A

As shown in Fig. 3, the symmetric stretching vibration peaks of C–N bond and C=O bond in PSI are at 1400 cm^{-1} and 1716 cm^{-1} , respectively. PASP-ED₂A shows the stretching vibration peaks of N–H, C=O and C–N in the amide bond at 3393 cm^{-1} , 1621 cm^{-1} and 1401 cm^{-1} . Noticeably, the dramatic change of vibration peak of carbonyl group from 1716 cm^{-1} (with broad signal) can be attributed to the fact that

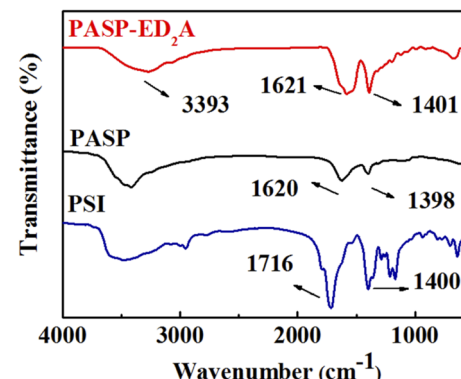


Fig. 3 FTIR spectra of PSI, PASP and PASP-ED₂A.

the formation of extra amide bond *via* ring-opening aminolysis. This is very similar to PASP (with two dramatic peaks at 1620 and 1398 cm^{-1}), indicating that PSI reacts with ED₂A to generate PASP-ED₂A.

Fig. 4 shows the ¹H NMR spectra of ED₂A, PASP and PASP-ED₂A in D_2O . The two absorbance peaks of $-\text{CH}_2-$ in ED₂A with an integration rate of 1 : 1 appear at 2.50 ppm and 3.10 ppm (Fig. 4(a)), which indicates that ED₂A is successfully synthesized. As depicted in Fig. 4(b), the broad peaks of $-\text{CH}-$ and $-\text{CH}_2-$ of PASP molecular chain emerge at 2.60 ppm and 4.30 ppm (with an integration ratio of 2 : 1), respectively. Besides, aside from the $-\text{CH}-$ and $-\text{CH}_2-$ peaks of PASP, the as-synthesized PASP-ED₂A shows the peaks of $-\text{CH}_2-$ in ED₂A at 3.50 ppm and 3.80 ppm (Fig. 4(c)). These data can further confirm the successful synthesis of PASP-ED₂A derivative.

3.2 Scale inhibition efficiency towards CaCO_3 and CaSO_4

Fig. 5(a) shows the scale inhibition efficiency-concentration curves of PASP and PASP-ED₂A towards CaCO_3 . In general, the scale inhibition efficiency of both scale inhibitors increases with the increase of their concentration and remains nearly unchanged at a certain concentration, showing an obvious “threshold effect”.³⁰ Particularly, PASP-ED₂A exhibits better

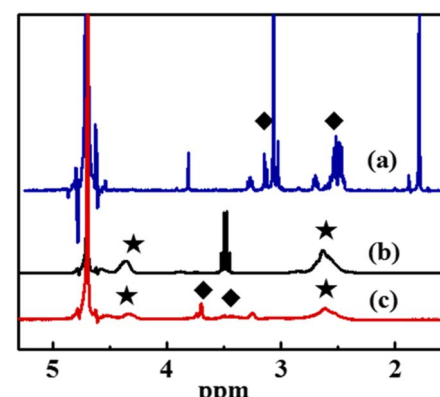


Fig. 4 ¹H NMR spectra of (a) ED₂A, (b) PASP and (c) PASP-ED₂A in D_2O .



scale inhibition performance against CaCO_3 than PASP, especially at a low concentration of 5 mg L^{-1} . This indicates that the introduction of coordination group-containing species into the side chain of PASP molecule contributes to greatly improving its scale inhibition performance. The reason might lie in that the coordination atoms of PASP-ED₂A molecule can chelate with free Ca^{2+} in water to inhibit its sedimentation therein.

Since the test temperature has an important influence on the scale inhibition performance of scale inhibitor,^{5,31,32} the scale inhibition performance of PASP and PASP-ED₂A is further evaluated in the test temperature range of $40\text{--}80^\circ\text{C}$. As can be seen from Fig. 5(b), the scale inhibition efficiency of PASP and PASP-ED₂A towards CaCO_3 decreases with the increase of temperature; and the scale inhibition efficiency of PASP-ED₂A is higher than that of PASP in the whole temperature range. For example, the scale inhibition efficiency of PASP decreases from 75.3% to 49.0% as the test temperature rises from 40°C to 80°C . Differing from PASP, the as-synthesized PASP-ED₂A maintains a high inhibition efficiency of 100% at $40\text{--}50^\circ\text{C}$, although the solubility of CaCO_3 decreases with increasing temperature. Fig. 5(c) shows the inhibition efficiency-time curves of PASP and PASP-ED₂A towards CaCO_3 scale. The scale inhibition efficiency of PASP-ED₂A decreases slowly with the extension of test time and is generally higher than that of PASP. Besides, PASP-ED₂A retains a scale inhibition efficiency of 57.1% after 12 h of scale inhibition test, which indicates that PASP-ED₂A has good time adaptability.

Fig. 6 shows the variations of the inhibition efficiency of PASP and PASP-ED₂A towards CaSO_4 scale with inhibitor

concentration as well as test temperature and time. As shown in Fig. 6(a), the scale inhibition efficiency of PASP and PASP-ED₂A increases sharply with increasing inhibitor concentration in the range of $1\text{--}6 \text{ mg L}^{-1}$. This is because the increase of the inhibitor concentration refers to the increase of the amount of scale inhibition molecules in the solution and to the augmented coordination probability of Ca^{2+} by the inhibitor.

Fig. 6(b) shows the influence of test temperature on the scale inhibition efficiency. The scale inhibition efficiency of PASP and PASP-ED₂A decreases significantly with the increase of temperature, which is because the crystallization rate of CaSO_4 scale increases rapidly therewith; and PASP-ED₂A exhibits a scale inhibition efficiency of 42.7% even at 90°C , much higher than that of PASP (only 24.2%).

Fig. 6(c) shows the variation of the inhibition efficiency of PASP-ED₂A and PASP against CaSO_4 scale with test time. With the extension of time, the scale inhibition efficiency of PASP gradually decreases, and the scale inhibition efficiency of PASP-ED₂A still remains at 100% even after 24 h of inhibition test. This indicates that PASP-ED₂A has excellent resistance against CaSO_4 scale.

3.3 Characterization of CaCO_3 and CaSO_4 scales

The SEM images of CaCO_3 crystals in the absence and presence of the scale inhibitors are shown in Fig. 7. In the absence of the scale inhibitors, the CaCO_3 crystal exhibits a very regular cubic structure. After adding PASP, the crystal structure of CaCO_3 is destroyed; and its surface morphology becomes irregular while

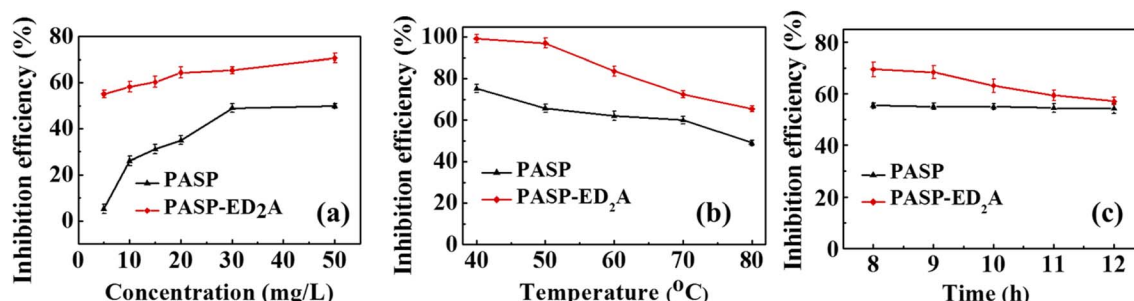


Fig. 5 Inhibition efficiency of PASP-ED₂A and PASP towards CaCO_3 scale versus (a) inhibitor concentration, (b) test temperature, and (c) test time.

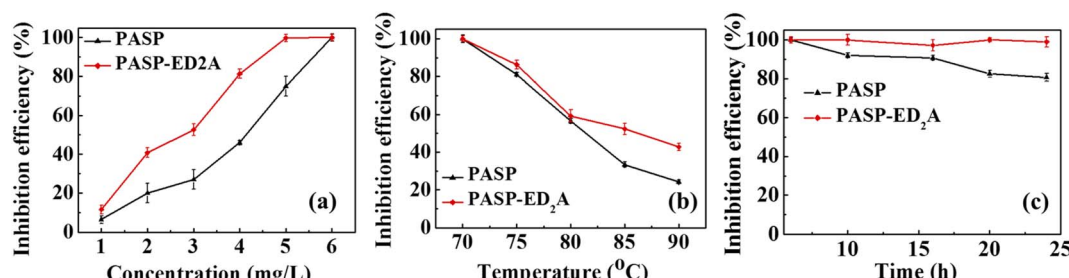


Fig. 6 Inhibition efficiency of PASP-ED₂A and PASP towards CaSO_4 scale versus (a) inhibitor concentration, (b) test temperature, and (c) test time.



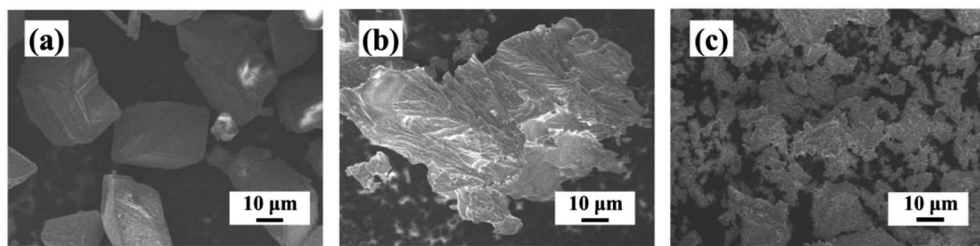


Fig. 7 SEM images of CaCO_3 : (a) without scale inhibitor, (b) with 30 mg L^{-1} PASP, and (c) with 30 mg L^{-1} PASP- ED_2A .

its structure becomes loose in association with the increase of particle size. After the addition of PASP- ED_2A , the CaCO_3 crystal appears as loose small particles with good access to dispersion. This could be because, on the one hand, the coordination groups in the molecular structure of PASP- ED_2A can chelate with Ca^{2+} , thereby inhibiting the production of CaCO_3 crystal. On the other hand, PASP- ED_2A can be adsorbed on the surface of CaCO_3 crystal, thereby inhibiting its regular growth and adding to its looseness. At the same time, the scale inhibitor molecules with negative charge adsorbed on the surface of CaCO_3 crystal could contribute to preventing the aggregation of CaCO_3 particles, thereby yielding CaCO_3 crystal with a reduced size.

Fig. 8 shows the SEM images of CaSO_4 scales in the absence and presence of the scale inhibitors. In the absence of the agent, CaSO_4 scale crystal presents a typical rectangular and tetragonal

structure. After the addition of PASP, the surface of CaSO_4 scale crystal becomes smooth. After the addition of PASP- ED_2A , CaSO_4 scale crystals grow into short rods and the surface becomes very rough. This may be due to the adsorption of PASP- ED_2A on the surface of scale crystal, which leads to the change of scale morphology.

The effect of the scale inhibitor on the crystal structure of CaCO_3 and CaSO_4 scales is investigated by XRD. Fig. 9(A) shows the XRD patterns of CaCO_3 scale without and with the addition of PASP and PASP- ED_2A . The CaCO_3 scale formed in the absence of the scale inhibitors mainly consists of calcite and aragonite. After the addition of PASP, the characteristic diffraction peaks of vaterite appear, and those of aragonite almost disappear. This indicates that the CaCO_3 scale formed in the presence of PASP mainly consists of calcite and vaterite. After the addition of PASP- ED_2A , the characteristic diffraction

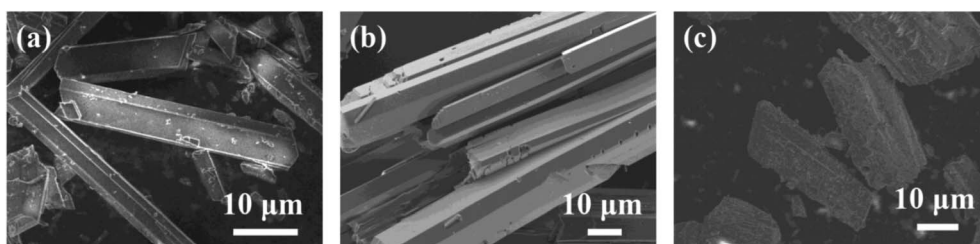


Fig. 8 SEM images of CaSO_4 : (a) without the scale inhibitor, (b) with 4 mg L^{-1} PASP, and (c) with 4 mg L^{-1} PASP- ED_2A .

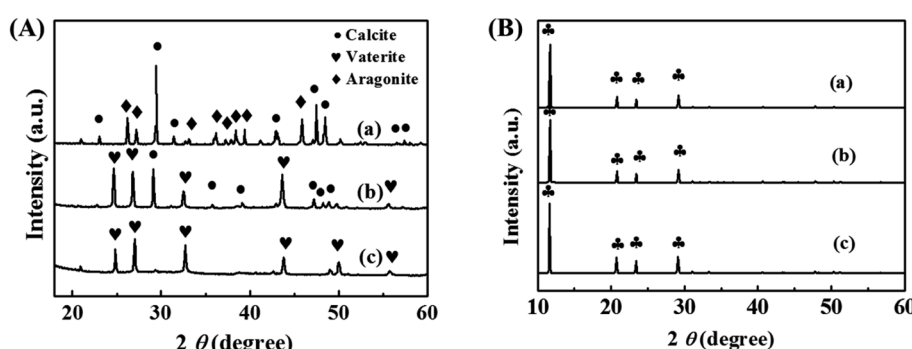


Fig. 9 XRD patterns of CaCO_3 scales formed in (A) aqueous solution of CaCO_3 ((a) without the scale inhibitor, (b) with 30 mg L^{-1} PASP, and (c) with 30 mg L^{-1} PASP- ED_2A) and (B) aqueous solution of CaSO_4 ((a) without the scale inhibitor, (b) with 4 mg L^{-1} PASP, and (c) with 4 mg L^{-1} PASP- ED_2A).



peak of the (110) facet of calcite disappears completely, possibly because the PASP-ED₂A molecules adsorbed on the surface of CaCO₃ particles *via* coordination contribute to effectively inhibiting the growth of CaCO₃ crystal along the (110) plane.^{5,33-35} Therefore, the main configuration of calcium carbonate is vaterite after the addition of PASP-ED₂A.

Fig. 9(B) shows the XRD patterns of CaSO₄ scale after adding PASP and PASP-ED₂A. It can be seen that the main crystal type of CaSO₄ scale formed without the addition of the scale inhibitors is gypsum (CaSO₄·2H₂O); and the crystal pattern of CaSO₄ scale obtained after the addition of PASP and PASP-ED₂A remains unchanged. This, in combination with corresponding SEM analysis, demonstrates that the scale inhibitor PASP-ED₂A can change the surface morphology of CaSO₄ scale but has no influence on its crystal type.^{7,33,36,37}

Fig. 10 shows the Ca 2p-XPS spectra of CaCO₃ scales obtained with and without the addition of the scale inhibitors. The addition of PASP and PASP-ED₂A leads to shift of the Ca 2p_{1/2} and Ca 2p_{3/2} peaks towards the low binding energy side by 0.18 eV and 0.30 eV, respectively. This indicates that PASP-ED₂A can more strongly influence the chemical environment of Ca²⁺ in CaCO₃ scale than PASP, which could be because PASP-ED₂A is easier to dwell on the surface of CaCO₃ *via* coordination adsorption.

Fig. 11 shows the Ca 2p-XPS spectra of CaSO₄ scales obtained with and without the addition of the scale inhibitors. The CaSO₄ scale obtained without the addition of the scale inhibitors shows Ca 2p_{1/2} and Ca 2p_{3/2} peaks at 351.16 eV and 347.62 eV, respectively. After the addition of PASP and PASP-ED₂A, the Ca

2p peaks shift towards high binding energy side by 0.32 eV and 0.44 eV, respectively. Here PASP and PASP-ED₂A still can cause changes in the chemical environment of Ca²⁺ in CaSO₄ scale, and PASP-ED₂A is superior to PASP in this sense.

3.4 Monitoring crystallization process of CaCO₃ and CaSO₄ scales

Fig. 12 shows the pH-time curves of the CaCO₃ solutions without and with the scale inhibitors (4 mg L⁻¹). The pH values of the blank CaCO₃ solution and the solution with PASP decrease rapidly in the early stage of inhibition tests and stabilize around a test duration of 5 min (blank CaCO₃ solution) or 10 min (CaCO₃ solutions with PASP). After the addition of PASP-ED₂A, the pH value varies at significantly slowed-down pace and reaches stabilization at greatly extended test duration. Table 1 shows the *t*_{ind} of CaCO₃ in the presence of different scale inhibitors. In 0.015 mol L⁻¹ CaCO₃ solution, PASP-ED₂A can increase the *t*_{ind} to 131.75 min, which indicates that PASP-ED₂A is superior to PASP in inhibiting the generation of CaCO₃ scale. Besides, the CaCO₃ crystals formed in the blank CaCO₃ solution and the CaCO₃ solutions with PASP or PASP-ED₂A exhibit surface energies of 44.3 mJ m⁻², 46.2 mJ m⁻² and 60.4 mJ m⁻², respectively (Fig. 12(d)). This demonstrates that the addition of PASP-ED₂A can significantly increase the surface energy of CaCO₃ crystal and reduce the nucleation rate of CaCO₃ scale, thereby exerting greatly improved scale inhibition performance.

Fig. 13 shows the conductivity-time curves of CaSO₄ solutions with and without scale inhibitors (0.75 mg L⁻¹ PASP or

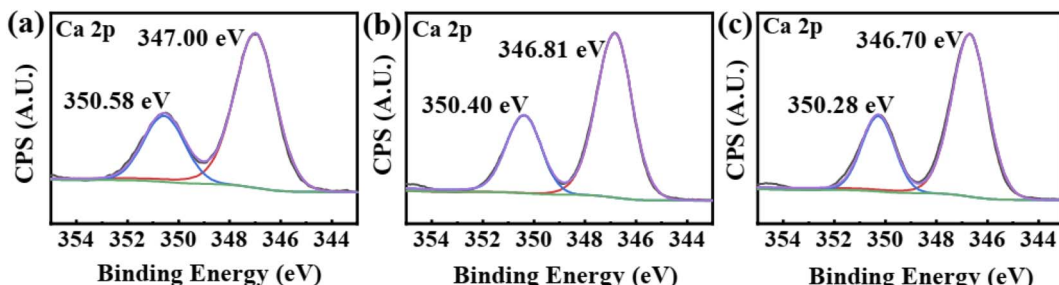


Fig. 10 XPS spectra of Ca 2p in CaCO₃ with different scale inhibitor. (a) Without antiscalant (b) with 30 mg L⁻¹ PASP (c) with 30 mg L⁻¹ PASP-ED₂A.

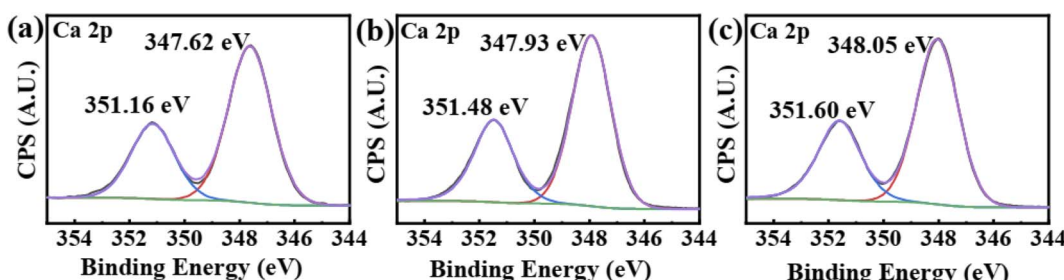


Fig. 11 XPS spectra of Ca 2p in CaSO₄ with different scale inhibitor. (a) Without antiscalant (b) with 4 mg L⁻¹ PASP (c) with 4 mg L⁻¹ PASP-ED₂A.



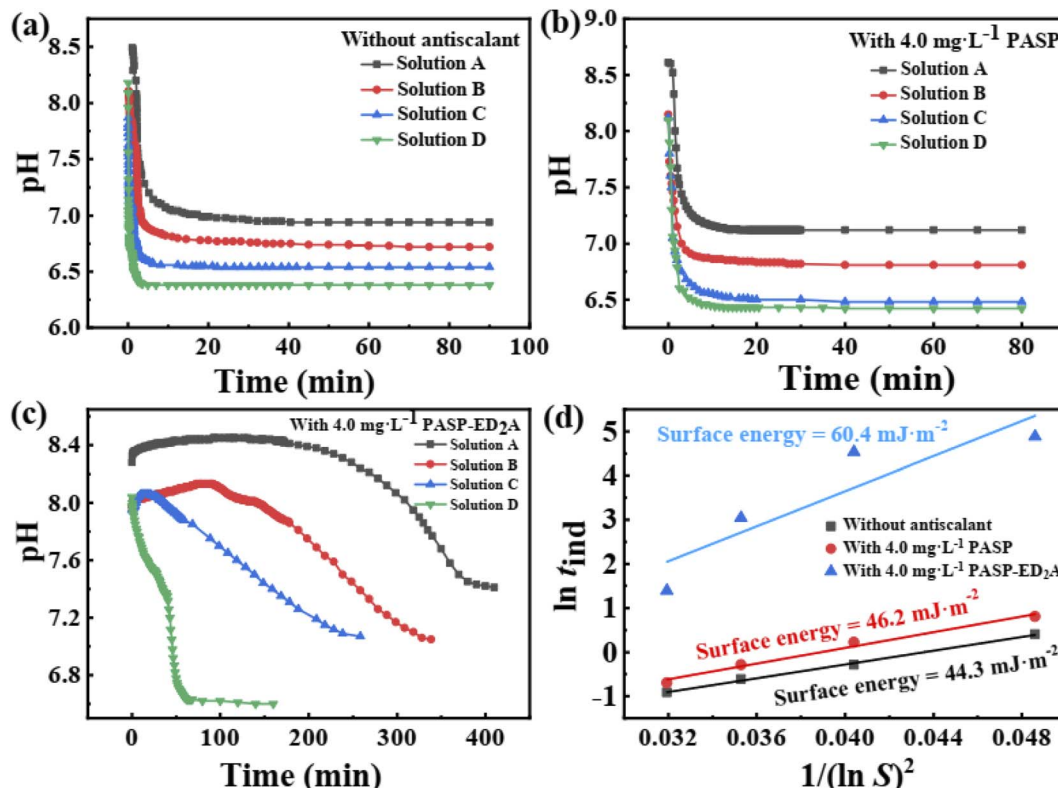


Fig. 12 pH–time curves of (a) blank CaCO_3 solution and the solutions with (b) 4.0 mg L^{-1} PASP and (c) 4.0 mg L^{-1} PASP–ED₂A as well as (d) relation between $\ln t_{\text{ind}}$ and $1/(\ln S)^2$ with or without the scale inhibitors.

PASP–ED₂A). The conductivity–time curve can determine the t_{ind} of CaSO_4 scale and the t_{ind} value can reflect the scale inhibition performance of the scale inhibitors. The larger the t_{ind} is, the lower the nucleation rate of CaSO_4 crystal would be, and the longer the time of crystal nucleus formation and growth would be. When the concentration of blank CaSO_4 solution and those CaSO_4 solutions with different scale inhibitors gradually increases from 0.07 mol L^{-1} to 0.10 mol L^{-1} , their conductivity tends to increase at different paces and level off at different test durations, while their t_{ind} tends to decrease therewith at different paces (Fig. 13 and Table 2). Particularly, the CaSO_4 solutions with PASP–ED₂A exhibit much larger t_{ind} than the blank CaSO_4 solution and the CaSO_4 solutions with PASP. This corresponds to the better scale inhibition performance of PASP–ED₂A in comparison to that of PASP.

Table 1 Induction time of pH test of CaCO_3 solutions with and without scale inhibitors

Category	Antiscalant	CaCO ₃ solutions with different concentration (mol L^{-1})			
		0.015	0.020	0.025	0.030
t_{ind} (min)	Blank	1.50	0.75	0.54	0.40
	PASP	2.25	1.25	0.75	0.50
	PASP–ED ₂ A	131.75	92.50	21.00	4.00

Table 2 Induction time of CaSO_4 solutions upon conductivity tests with and without scale inhibitors

Category	Antiscalant	CaSO ₄ solutions with different concentration (mol L^{-1})			
		0.07	0.08	0.09	0.10
t_{ind} (min)	Blank	5.0	2.8	1.5	1.0
	PASP	12.5	4.8	3.0	2.0
	PASP–ED ₂ A	31.0	12.5	3.3	2.3

Table 2 shows the t_{ind} of CaSO_4 in the presence of different scale inhibitors. In 0.07 mol L^{-1} CaSO_4 solution, PASP can increase the induction time from 5.0 min to 12.5 min, while PASP–ED₂A can increase the induction time to 31.0 min. This indicates that compared with PASP, the PASP–ED₂A derivative can more efficiently inhibit the growth of CaSO_4 scale. As can be seen from Fig. 13(d), the CaSO_4 crystals formed in the blank CaSO_4 solution and the CaSO_4 solutions with 0.75 mg L^{-1} PASP or 0.75 mg L^{-1} PASP–ED₂A exhibit surface energies of 14.8 eV, 15.4 eV and 17.7 eV, respectively. The increase in the surface energy of CaSO_4 crystal upon the addition of PASP–ED₂A demonstrates that PASP–ED₂A can well retard the formation and growth of CaSO_4 crystal nuclei, thereby exerting improved scale inhibition performance.

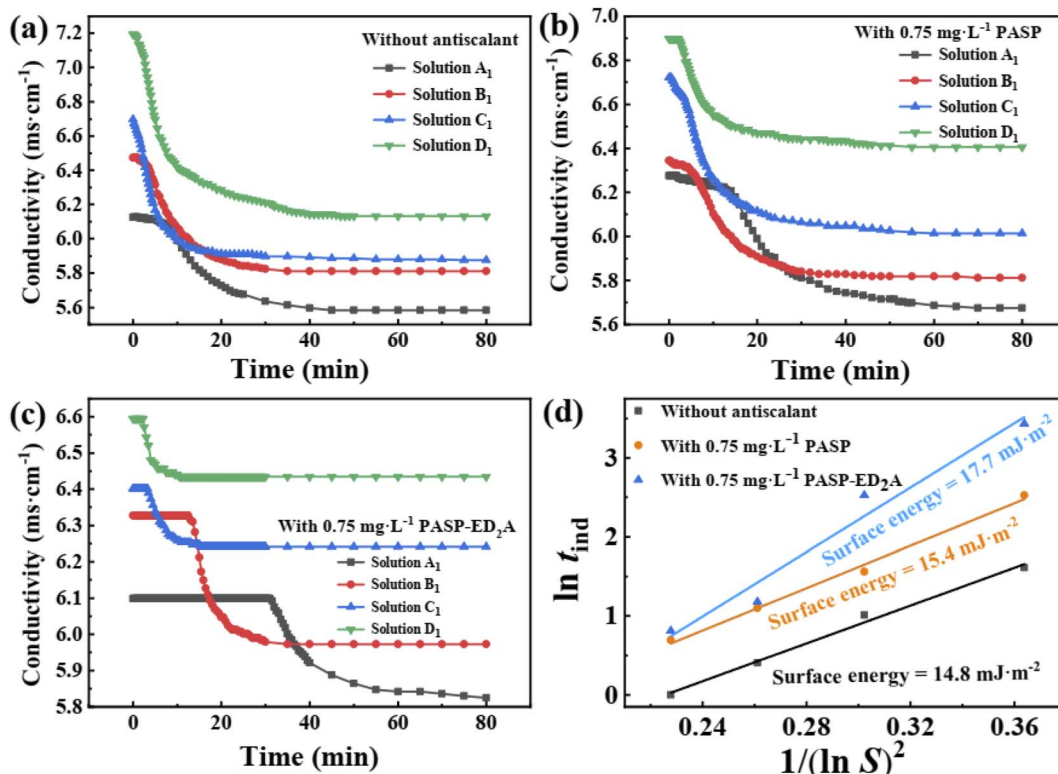


Fig. 13 Conductivity–time curves of CaSO_4 crystals formed without antiscalant (a), with 0.75 mg L^{-1} PASP (b), and with 0.75 mg L^{-1} PASP–ED₂A (c), as well as relation between $\ln t_{\text{ind}}$ and $1/(\ln S)^2$ with and without scale inhibitors (d).

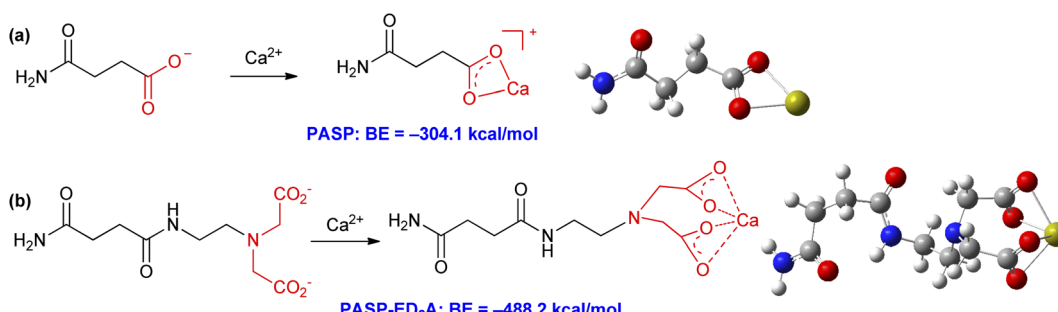


Fig. 14 Binding energies for chelation.

3.5 Theoretical calculation results of Pasp and Pasp-ED₂A

From the above discussion, it can be seen that Pasp and Pasp-ED₂A can exert their scale inhibition effect by chelating with Ca^{2+} . To better understand the coordination details, we further investigate their chelating ability with Ca^{2+} by DFT calculations (for details, please see ESI†). Fig. 14 shows the binding energies (BE) for Pasp and Pasp-ED₂A to chelate with Ca^{2+} . The carboxyl groups in the side chains of Pasp and Pasp-ED₂A can chelate with Ca^{2+} to form one or two four-membered rings, respectively; and the binding energies for Pasp– Ca^{2+} chelation and Pasp-ED₂A– Ca^{2+} chelation are $-304.1 \text{ kcal mol}^{-1}$ and $-488.2 \text{ kcal mol}^{-1}$, respectively. This means that, as compared with Pasp, the Pasp-ED₂A

derivative is easier to combine with Ca^{2+} , thereby exerting better scale inhibition performance.

4. Conclusions

In summary, a novel phosphorus-free Pasp derivative with side chains bearing semi-EDTA structure is rationally designed and successfully prepared. Static scale inhibition tests demonstrate that the as-prepared Pasp-ED₂A derivative exhibits good scale inhibition performance against CaCO_3 and CaSO_4 at a low concentration or a high temperature; and it exhibits better scale inhibition performance than Pasp. SEM and XRD characterizations demonstrate that the addition of Pasp-ED₂A can affect



the morphology of CaCO_3 and CaSO_4 as well as the crystal shape of CaCO_3 . Namely, PASP-ED₂A can promote the formation of vaterite crystal and delay the formation of calcite crystal. This is because the coordination atoms in the molecular structure of PASP-ED₂A can chelate with Ca^{2+} , thereby inhibiting the combination of Ca^{2+} with anions and preventing the generation of CaCO_3 scale or CaSO_4 scale. XPS analyses indicate that PASP and PASP-ED₂A can change the chemical environment of Ca^{2+} to different extents, which could partly account for the difference in their scale inhibition performance. Besides, monitoring crystallization processes of CaCO_3 and CaSO_4 crystals in association with DFT calculations reveals that the CaCO_3 and CaSO_4 crystals generated in the presence of PASP-ED₂A exhibit significantly increased surface energy, while PASP-ED₂A is easier than PASP to chelate with Ca^{2+} . In other words, the PASP-ED₂A derivative can more efficiently retard the formation and growth of CaCO_3 and CaSO_4 crystal nuclei, thereby exerting better inhibition performance against CaCO_3 and CaSO_4 scales than PASP. Further studies towards the development of other novel PASP derivatives are ongoing in our laboratories.

Conflicts of interest

There are no conflicts to declare.

References

- 1 X. Qu, P. J. J. Alvarez and Q. Li, Applications of nanotechnology in water and wastewater treatment, *Water Res.*, 2013, **47**, 3931–3946, DOI: [10.1016/j.watres.2012.09.058](https://doi.org/10.1016/j.watres.2012.09.058).
- 2 A. Zeino, I. Abdulazeez, M. Khaled, M. W. Jawich and I. B. Obot, Mechanistic study of polyaspartic acid (PASP) as eco-friendly corrosion inhibitor on mild steel in 3% NaCl aerated solution, *J. Mol. Liq.*, 2018, **250**, 50–62, DOI: [10.1016/j.molliq.2017.11.160](https://doi.org/10.1016/j.molliq.2017.11.160).
- 3 Y. Zhou, J. Wang and Y. Fang, Green and high effective scale inhibitor based on ring-opening graft modification of polyaspartic acid, *Catalysts*, 2021, **11**, DOI: [10.3390/catal11070802](https://doi.org/10.3390/catal11070802).
- 4 X. Li, B. Gao, Q. Yue, D. Ma, H. Rong, P. Zhao and P. Teng, Effect of six kinds of scale inhibitors on calcium carbonate precipitation in high salinity wastewater at high temperatures, *J. Environ. Sci.*, 2015, **29**, 124–130, DOI: [10.1016/j.jes.2014.09.027](https://doi.org/10.1016/j.jes.2014.09.027).
- 5 W. Yu, D. Song, W. Chen and H. Yang, Antiscalants in RO membrane scaling control, *Water Res.*, 2020, **183**, 115985, DOI: [10.1016/j.watres.2020.115985](https://doi.org/10.1016/j.watres.2020.115985).
- 6 H. Zhang, X. Luo, X. Lin, P. Tang, X. Lu, M. Yang and Y. Tang, Biodegradable carboxymethyl inulin as a scale inhibitor for calcite crystal growth: molecular level understanding, *Desalination*, 2016, **381**, 1–7, DOI: [10.1016/j.desal.2015.11.029](https://doi.org/10.1016/j.desal.2015.11.029).
- 7 S. Zhang, H. Qu, Z. Yang, C. Fu, Z. Tian and W. Yang, Scale inhibition performance and mechanism of sulfamic/amino acids modified polyaspartic acid against calcium sulfate, *Desalination*, 2017, **419**, 152–159, DOI: [10.1016/j.desal.2017.06.016](https://doi.org/10.1016/j.desal.2017.06.016).
- 8 Y. Zhang, H. Yin, Q. Zhang, Y. Li and P. Yao, Synthesis and characterization of novel polyaspartic acid/urea graft copolymer with acylamino group and its scale inhibition performance, *Desalination*, 2016, **395**, 92–98, DOI: [10.1016/j.desal.2016.05.020](https://doi.org/10.1016/j.desal.2016.05.020).
- 9 J. Chen, L. Xu, J. Han, M. Su and Q. Wu, Synthesis of modified polyaspartic acid and evaluation of its scale inhibition and dispersion capacity, *Desalination*, 2015, **358**, 42–48, DOI: [10.1016/j.desal.2014.11.010](https://doi.org/10.1016/j.desal.2014.11.010).
- 10 V. Fischer, K. Landfester and R. Muñoz-Espí, Stabilization of calcium oxalate metastable phases by oligo(L-glutamic acid): effect of peptide chain length, *Cryst. Growth Des.*, 2011, **11**, 1880–1890, DOI: [10.1021/cg200058d](https://doi.org/10.1021/cg200058d).
- 11 M. Ø. Olderøy, M. Xie, B. L. Strand, E. M. Flaten, P. Sikorski and J.-P. Andreassen, Growth and nucleation of calcium carbonate vaterite crystals in presence of alginate, *Cryst. Growth Des.*, 2009, **9**, 5176–5183, DOI: [10.1021/cg9005604](https://doi.org/10.1021/cg9005604).
- 12 D.-E. Liu, H. Han, H. Lu, G. Wu, Y. Wang, J. Ma and H. Gao, Synthesis of amphiphilic polyaspartamide derivatives and construction of reverse micelles, *RSC Adv.*, 2014, **4**, 37130–37137, DOI: [10.1039/C4RA04432K](https://doi.org/10.1039/C4RA04432K).
- 13 Y. Lu, M. Chau, A. J. Boyle, P. Liu, A. Niehoff, D. Weinrich, R. M. Reilly and M. A. Winnik, Effect of pendant group structure on the hydrolytic stability of polyaspartamide polymers under physiological conditions, *Biomacromolecules*, 2012, **13**, 1296–1306, DOI: [10.1021/bm2018239](https://doi.org/10.1021/bm2018239).
- 14 X. Cheng, J. Liu, L. Wang, R. Wang, Z. Liu and R. Zhuo, An enzyme-mediated in situ hydrogel based on polyaspartamide derivatives for localized drug delivery and 3D scaffolds, *RSC Adv.*, 2016, **6**, 101334–101346, DOI: [10.1039/C6RA18479K](https://doi.org/10.1039/C6RA18479K).
- 15 E. Jalalvandi, L. R. Hanton and S. C. Moratti, Schiff-base based hydrogels as degradable platforms for hydrophobic drug delivery, *Eur. Polym. J.*, 2017, **90**, 13–24, DOI: [10.1016/j.eurpolymj.2017.03.003](https://doi.org/10.1016/j.eurpolymj.2017.03.003).
- 16 D. Juriga, K. Nagy, A. Jedlovszky-Hajdu, K. Perczel-Kovách, Y. M. Chen, G. Varga and M. Zrínyi, Biodegradation and osteosarcoma cell cultivation on poly(aspartic acid) based hydrogels, *ACS Appl. Mater. Interfaces*, 2016, **8**, 23463–23476, DOI: [10.1021/acsami.6b06489](https://doi.org/10.1021/acsami.6b06489).
- 17 Y. Gao, L. Fan, L. Ward and Z. Liu, Synthesis of polyaspartic acid derivative and evaluation of its corrosion and scale inhibition performance in seawater utilization, *Desalination*, 2015, **365**, 220–226, DOI: [10.1016/j.desal.2015.03.006](https://doi.org/10.1016/j.desal.2015.03.006).
- 18 J. Yang, T. Liu, H. Liu, D. Zhang, L. Zhai, J. Liu, M. Wang, Y. Chen, B. Chen and H. Wang, Biodegradable PASP can effectively inhibit nitrification, moderate NH_3 emission, and promote crop yield, *Arch. Agron. Soil Sci.*, 2019, **65**, 1273–1286, DOI: [10.1080/03650340.2018.1562275](https://doi.org/10.1080/03650340.2018.1562275).
- 19 M. F. Mady, A. Rehman and M. A. Kelland, Synthesis and study of modified polyaspartic acid coupled phosphonate and sulfonate moieties as green oilfield scale inhibitors, *Ind. Eng. Chem. Res.*, 2021, **60**, 8331–8339, DOI: [10.1021/acs.iecr.1c01473](https://doi.org/10.1021/acs.iecr.1c01473).



- 20 Z. Amjad and P. G. Koutsoukos, Evaluation of maleic acid based polymers as scale inhibitors and dispersants for industrial water applications, *Desalination*, 2014, **335**, 55–63, DOI: [10.1016/j.desal.2013.12.012](https://doi.org/10.1016/j.desal.2013.12.012).
- 21 S. Carvalho, L. Palermo, L. Boak, K. Sorbie and E. F. Lucas, Influence of terpolymer based on amide, carboxylic, and sulfonic groups on the barium sulfate inhibition, *Energy Fuels*, 2017, **31**, 10648–10654, DOI: [10.1021/acs.energyfuels.7b01767](https://doi.org/10.1021/acs.energyfuels.7b01767).
- 22 M. A. Migahed, S. M. Rashwan, M. M. Kamel and R. E. Habib, Synthesis, characterization of polyaspartic acid-glycine adduct and evaluation of their performance as scale and corrosion inhibitor in desalination water plants, *J. Mol. Liq.*, 2016, **224**, 849–858, DOI: [10.1016/j.molliq.2016.10.091](https://doi.org/10.1016/j.molliq.2016.10.091).
- 23 G. McLendon, R. J. Motekaitis and A. E. Martell, Cobalt complexes of ethylenediamine-N,N'-diacetic acid and ethylenediamine-N,N'-diacetic acid: two-nitrogen oxygen carriers, *Inorg. Chem.*, 1975, **14**, 1993–1996, DOI: [10.1021/ic50150a050](https://doi.org/10.1021/ic50150a050).
- 24 M. Chaussemier, E. Pourmohtasham, D. Gelus, N. Pécul, H. Perrot, J. Lédion, H. Cheap-Charpentier and O. Horner, State of art of natural inhibitors of calcium carbonate scaling. A review article, *Desalination*, 2015, **356**, 47–55, DOI: [10.1016/j.desal.2014.10.014](https://doi.org/10.1016/j.desal.2014.10.014).
- 25 E. A. Abdel-Aal, H. M. Abdel-Ghafar and B. E. El Anadouli, New findings about nucleation and crystal growth of reverse osmosis desalination scales with and without Inhibitor, *Cryst. Growth Des.*, 2015, **15**, 5133–5137, DOI: [10.1021/acs.cgd.5b01091](https://doi.org/10.1021/acs.cgd.5b01091).
- 26 Q. Liu, G.-R. Xu and R. Das, Inorganic scaling in reverse osmosis (RO) desalination: Mechanisms, monitoring, and inhibition strategies, *Desalination*, 2019, **468**, 114065, DOI: [10.1016/j.desal.2019.07.005](https://doi.org/10.1016/j.desal.2019.07.005).
- 27 D. Hasson, A. Drak and R. Semiat, Inception of CaSO_4 scaling on RO membranes at various water recovery levels, *Desalination*, 2001, **139**, 73–81, DOI: [10.1016/S0011-9164\(01\)00296-X](https://doi.org/10.1016/S0011-9164(01)00296-X).
- 28 D. Hasson, A. Drak and R. Semiat, Induction times induced in an RO system by antiscalants delaying CaSO_4 precipitation, *Desalination*, 2003, **157**, 193–207, DOI: [10.1016/S0011-9164\(03\)00399-0](https://doi.org/10.1016/S0011-9164(03)00399-0).
- 29 W. Yu, W. Chen and H. Yang, Evaluation of structural effects on the antiscaling performance of various graft cellulose-based antiscalants in RO membrane scaling control, *J. Membr. Sci.*, 2021, **620**, 118893, DOI: [10.1016/j.memsci.2020.118893](https://doi.org/10.1016/j.memsci.2020.118893).
- 30 Y. Zuo, Y. Sun, W. Yang, K. Zhang, Y. Chen, X. Yin and Y. Liu, Performance and mechanism of 1-hydroxy ethyldene-1,1-diphosphonic acid and 2-phosphonobutane-1,2,4-tricarboxylic acid in the inhibition of calcium carbonate scale, *J. Mol. Liq.*, 2021, **334**, 116093, DOI: [10.1016/j.molliq.2021.116093](https://doi.org/10.1016/j.molliq.2021.116093).
- 31 A. Jawor and E. M. V. Hoek, Effects of feed water temperature on inorganic fouling of brackish water RO membranes, *Desalination*, 2009, **235**, 44–57, DOI: [10.1016/j.desal.2008.07.004](https://doi.org/10.1016/j.desal.2008.07.004).
- 32 Y. Cheng, X. Guo, X. Zhao, Y. Wu, Z. Cao, Y. Cai and Y. Xu, Nanosilica modified with polyaspartic acid as an industrial circulating water scale inhibitor, *npj Clean Water*, 2021, **4**, DOI: [10.1038/s41545-021-00137-y](https://doi.org/10.1038/s41545-021-00137-y).
- 33 E. G. Darton, Membrane chemical research: centuries apart, *Desalination*, 2000, **132**, 121–131, DOI: [10.1016/S0011-9164\(00\)00141-7](https://doi.org/10.1016/S0011-9164(00)00141-7).
- 34 S. Kamali and R. Arefinia, Effect of PAAT as an environmentally friendly terpolymer on the scale inhibition of CaCO_3 in artificial seawater: chemical and electrochemical study, *Ind. Eng. Chem. Res.*, 2019, **59**, 627–635, DOI: [10.1021/acs.iecr.9b05943](https://doi.org/10.1021/acs.iecr.9b05943).
- 35 H. Li, M. K. Hsieh, S. H. Chien, J. D. Monnell, D. A. Dzombak and R. D. Vidic, Control of mineral scale deposition in cooling systems using secondary-treated municipal wastewater, *Water Res.*, 2011, **45**, 748–760, DOI: [10.1016/j.watres.2010.08.052](https://doi.org/10.1016/j.watres.2010.08.052).
- 36 Y. M. Al-Roomi and K. F. Hussain, Potential kinetic model for scaling and scale inhibition mechanism, *Desalination*, 2016, **393**, 186–195, DOI: [10.1016/j.desal.2015.07.025](https://doi.org/10.1016/j.desal.2015.07.025).
- 37 R. Ketrane, B. Saidani, O. Gil, L. Leleyter and F. Baraud, Efficiency of five scale inhibitors on calcium carbonate precipitation from hard water: Effect of temperature and concentration, *Desalination*, 2009, **249**, 1397–1404, DOI: [10.1016/j.desal.2009.06.013](https://doi.org/10.1016/j.desal.2009.06.013).

